A Study on Optimization of Wireless Power Transmission Ferrite-less Coils in the 85 kHz Band by Numerical Analysis

Yuto Yamada [1)] Takehiro Imura[1)]

1) Faculty of Science and Engineering, Tokyo University of Science, Noda, Chiba, Japan

E-mail: yuto.yamada20@gmail.com

ABSTRACT: Wireless Power Transfer (WPT) has received a great deal of attention in recent years. Wireless power transfer for Electric Vehicles (EV) is becoming more important as a key factor in the popularization of EVs. Although the efficiency of wireless power transfer by magnetic field resonance can be evaluated by the *kQ* product, the optimum coil design method that maximizes the *kQ* product at a specific frequency has not yet been established. In the previous research, it is very troublesome because the electromagnetic field analysis was repeated by trial and error. In this paper, the *kQ* product is modeled for the number of turns in the Test Stations GA-WPT1 and VA-WPT1/Z3, which are defined in the international standard SAE J2954, and the coil that achieves the maximum efficiency is evaluated in terms of the number of turns. Although some errors in the modeling of the *kQ* product are expected to occur, a high-efficiency coil design plan is presented with almost no errors in terms of efficiency.

KEY WORDS: electric vehicle, coil design, stationary wireless power transfer, coil optimization, numerical analysis,

1. INTRODUCTION

1.1 Background

Wireless power transmission to electric vehicles (EVs) has been attracting attention in recent years as a clue to the stagnation of EV penetration [1], [2]. EV penetration has been slow due to problems such as cost, lack of charging spots, and range. However, the weight and cost of the vehicle will increase. It has also been claimed that there is a shortage of resources used for the batteries themselves. In order to solve these problems, research is currently being done on wireless power transmission while the vehicle is running or stopped. In particular, wireless power transfer while driving is a very attractive technology that minimizes the size of the on-board battery and extends the cruising range to a semi-infinite level by embedding coils in the road and using coils mounted under the vehicle to supply power while driving [3] - [7].

In this paper, we are going to study stationary wireless power transfer, which has a high demand and a near-future of practical use. Coil design is a very important topic in WPT systems, although there are many issues such as coil cost, durability, weight, power, and efficiency.

1.2 Purpose

In this paper, the goal is to maximize the transmission efficiency of WPT by magnetic field resonant coupling in the S-S system. The maximum efficiency of the magnetic field resonant coupling η_{max} depends on the *kQ* product obtained from the coupling coefficient *k* of the transmitter and receiver coils and the quality factor *Q* value of the coil. The wireless power transfer efficiency η can be maximized by maximizing *kQ* product [8], but a coil design method that maximizes the *kQ* product at a specific frequency has not yet been established [9].

In previous studies, electromagnetic field analysis has been performed using FEM (Finite Element Method) [10] - [12], but it is very time-consuming because the coil parameters are successively changed and the optimal coil is sought by trial and error.

Hence, the optimal coil is obtained by numerical analysis using 4,000 strands of Litz wire, taking Test Station GA-WPT1 (Fig. 1) and Test Station VA-WPT1/Z3 (Fig. 2), which are specified in SAE J2954, as examples, assuming that the power is supplied to the EV while the vehicle is stationary [13]. In SAE J2954, ferrite is used, but in this study, optimization is performed without ferrite.

1.3 Structure of this paper

The equivalent circuit of magnetic field resonant coupling and the theory of transmission efficiency and *kQ* product are presented in Chapter 2, the proposed method and measurement results are shown in Chapter 3, misalignment is discussed in Chapter 4, and the conclusion is given in Chapter 5.

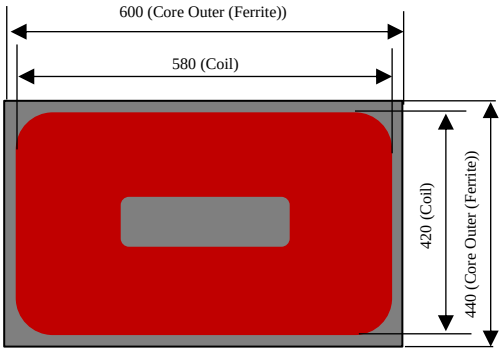

Fig. 1 Test station GA-WPT1

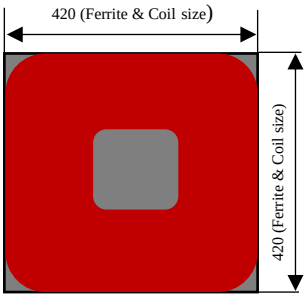

Fig. 2 Test station VA-WPT1/Z3

2. PRINCIPLE

2.1 Magnetic field resonant coupling

In this paper, we use the S-S method of magnetic field resonance coupling, in which a capacitor and an inductor are connected in series and resonate on both the primary (transmission side) and secondary (receiving side) sides for WPT in electric vehicles [14].

The equivalent circuit is shown in Fig. 3.

The resonant angular frequency ω_0 of the circuit can be shown using the self-inductances L_1 and L_2 and the resonant capacitors C_1 and C_2 as follows

$$\omega_0 = \frac{1}{\sqrt{L_1 C_1}} = \frac{1}{\sqrt{L_2 C_2}} \tag{1}$$

The coupling coefficient k and quality factor Q of the coil are shown below using the mutual inductance L_m and the internal resistance r_i of the coil (i= 1, 2).

$$k = \frac{L_m}{\sqrt{L_1 L_2}} \tag{2}$$

$$Q = \frac{\omega_0 L_i}{r_i} \tag{3}$$

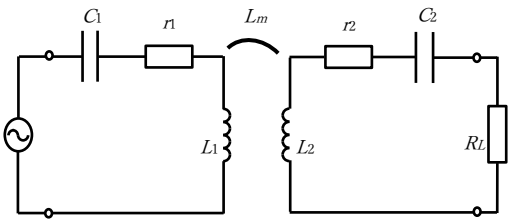

Fig. 3 Equivalent circuit in magnetic field resonance coupling of (S-S).

By using the optimum load resistance $R_{L,\eta max}$ that maximizes the efficiency η, the maximum efficiency η_{max} can be shown as follows.

$$R_{L,\eta max} = r_2\sqrt{1 + k^2 Q_1 Q_2} \tag{4}$$

$$\eta_{max} = \frac{k^2 Q_1 Q_2}{(1 + \sqrt{1 + k^2 Q_1 Q_2})^2} \tag{5}$$

From (2) and (3), the kQ product can be expressed in

$$k^2 Q_1 Q_2 = \frac{(\omega_0 L_m)^2}{r_1 r_2} \tag{6}$$

The relationship between kQ product and efficiency is shown in the Fig. 4. It can be seen that the maximum efficiency η_{max} can be increased by increasing the kQ product.

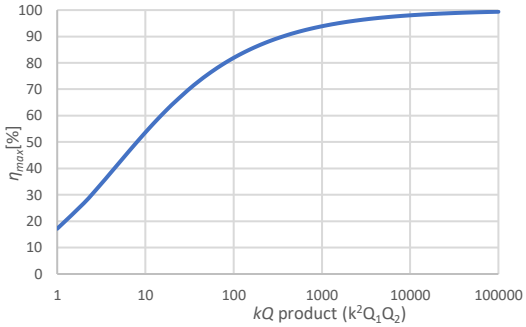

Fig. 4 Relationship between kQ product and maximum efficiency.

2.2 Parameters to evaluate

The resonant angular frequency ω_0 is known because the specified frequency band is 85 kHz. Therefore, in this study, the kQ product is obtained indirectly by deriving the mutual inductance L_m and the internal resistance r of the coil. MATLAB is mainly used for the analysis.

2.2.1 Mutual inductance L_m

The mutual inductance L_m is derived by the Neumann equation (7). The parameters used in the analysis are shown in Fig. 5.

$$L_m = \frac{\mu_0}{4\pi}\oint_{C1}\oint_{C2}\frac{dl_1 dl_2}{D} \tag{7}$$

2.2.2 Internal resistance r

When dealing with alternating current, there are two types of losses: the skin effect loss, which causes current to concentrate on the surface of the conductor, and the proximity effect loss, which causes a bias in the ease of current flow due to the magnetic field

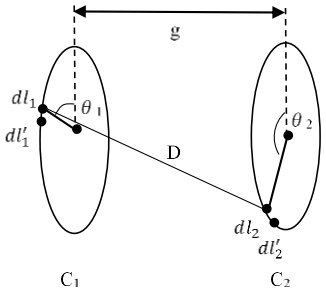

Fig. 5 Parameters of the Neumann equation

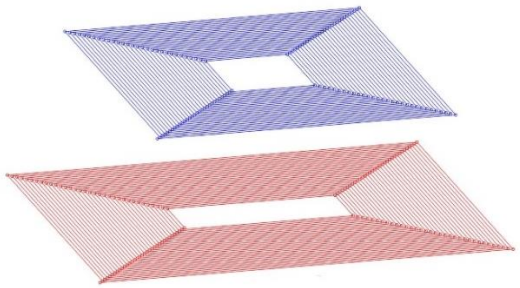

Fig. 6 Assumed coil model

between adjacent wires. In order to reduce the skin effect loss, Litz wire, which is a bundle of many thin strands, is mainly used in the kHz band. The equations for deriving the skin effect and proximity effect are shown below [15], [16]. In this case, there is no iron loss due to the air-core coil.

Skin effect loss:

$$P_{S,Litz} = n \cdot F_R(f) \cdot R_{DC} \cdot I_{rms}^2 \quad [\mathrm{W/m}] \tag{8}$$

Proximity effect loss:

$$P_{P,Litz} = n \cdot G_R(f) \cdot R_{DC} \cdot \left(H_e^2 + H_i^2\right) \quad [\mathrm{W/m}] \tag{9}$$

n, δ, R_{DC}, I_{rms}^2,F_R and G_R are shown below.

$$\text{Number of Litz wire strands} : n$$

$$\text{Epidermal depth} : \delta = \frac{1}{\sqrt{\pi \mu_0 \sigma f}}$$

$$\text{DC Resistance} : R_{DC} = \frac{4}{\sigma \pi d_i^2}$$

$$\xi = \frac{d_i}{\sqrt{2}\delta}$$

$$I_{rms}^2 = \frac{\hat{I}^2}{2n^2}$$

$$F_R = \frac{\xi}{2\sqrt{2}} \cdot \frac{1}{\mathrm{ber}_1(\xi)^2 + \mathrm{bei}_1(\xi)^2} \cdot \{-\mathrm{ber}_0(\xi)\mathrm{ber}_1(\xi) + \mathrm{ber}_0(\xi)\mathrm{bei}_1(\xi) - \mathrm{bei}_0(\xi)\mathrm{ber}_1(\xi) - \mathrm{bei}_0(\xi)\mathrm{bei}_1(\xi)\}$$

$$G_R = -\frac{\xi \pi^2 di^2}{2\sqrt{2}} \cdot \frac{1}{\mathrm{ber}_0(\xi)^2 + \mathrm{bei}_0(\xi)^2} \cdot \{\mathrm{ber}_2(\xi)\mathrm{ber}_1(\xi) + \mathrm{ber}_2(\xi)\mathrm{bei}_1(\xi) - \mathrm{bei}_2(\xi)\mathrm{ber}_1(\xi) + \mathrm{bei}_2(\xi)\mathrm{bei}_1(\xi)\}$$

The proximity effect due to the internal magnetic field H_i was calculated in MATLAB using the PEEC method, which is a method that enables numerical analysis by predictively converting electromagnetic problems into equivalent circuit problems [17].

The external magnetic field H_e is mainly the magnetic field due to the shape of the coil. For simplicity, only the adjacent Litz wires are considered, and the adjacent lines are assumed to be of infinite length and the current I is assumed to flow uniformly.

The external magnetic field H_e is shown below

$$H_e^2 = \frac{\hat{I}^2}{(2\pi d)^2} \tag{10}$$

By dividing equations (8) and (9) by $\hat{I}^2$ at the end, the internal resistance per unit length can be expressed by the equation. This equation includes the DC resistance.

$$r = \frac{\left(P_{S,Litz} + P_{P,Litz}\right)}{\hat{I}^2} \quad [\Omega/\mathrm{m}] \tag{11}$$

The parameters of the Litz wire used in the analysis are shown in Fig. 7. The structure of the Litz wire output by MATLAB is shown in Fig. 8.

3. PROPOSAL METHOD

In this section, we show the evaluation procedure and measurement results of *kQ* product. Five types of coils with different numbers of turns were made for each side of the power transmission and reception, and the analysis and measurement values were compared. The Fig. 9 and Fig. 10 shows some of the coils made and the measurement scene.

In this study, based on SAE J2954 Test Station GA-WPT1 and Test Station VA-WPT1/Z3, the Litz wire used and transmission distance are determined first, and then evaluated by the number of turns.

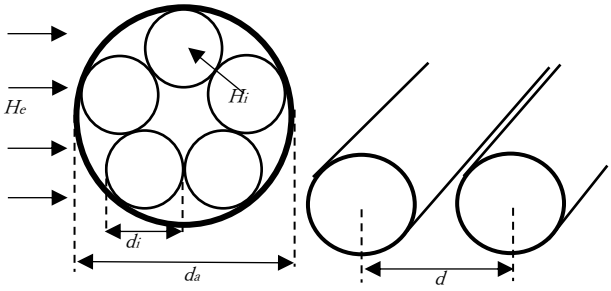

(a) External and internal magnetic fields (b) Pitch

Fig. 7 Litz wire parameter

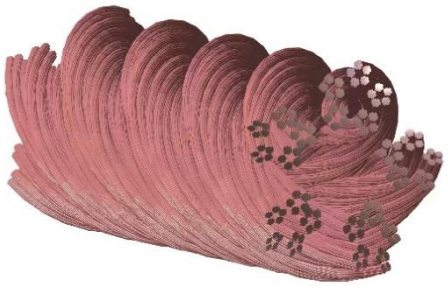

Fig. 8 Litz Wire (AWG44*4000(=32/5/5/5))

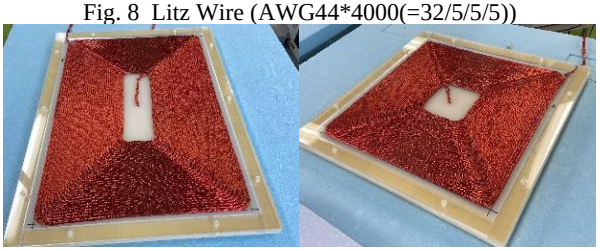

(a) Transmission side N_1=34 (b) Receiving side N_2=30

Fig. 9 Some of the coils used

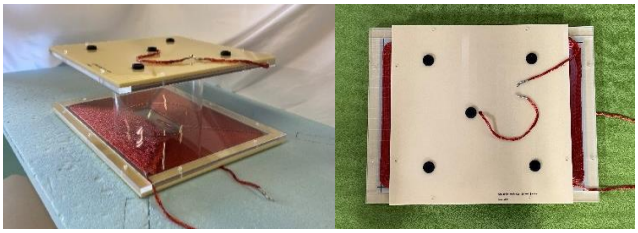

Fig. 10 Measurement scene (No misalignment)

3.1 STEP1

Determine the coil specifications based on the WPT environment to be optimized. Determine the gap, the Litz wire, the distance between wires, and the applicable frequency band.

The air gap was set to 200 mm, and AWG44/4000 was used as the Litz wire [18]. The distance between lines was set to $d = d_a$. The applicable frequency band was set to 85 kHz.

3.2 STEP2

The equation of the relationship between the number of turns N and the Litz wire length l is shown. The parameters of the coil are shown in Fig. 11. Using the number of turns N, coil size X, Y, Litz wire outer diameter d_a, and distance between wires α (= d - d_a), the Litz wire length l can be shown as follows

$$l = \{2X + 2Y + 4\alpha - 4(d_a + \alpha) \cdot N\} \cdot N - \alpha \qquad (12)$$

3.3 STEP3

The mutual inductance is derived for each combination of the number of turns of the primary (transmission side) and secondary (receiving side) coils.

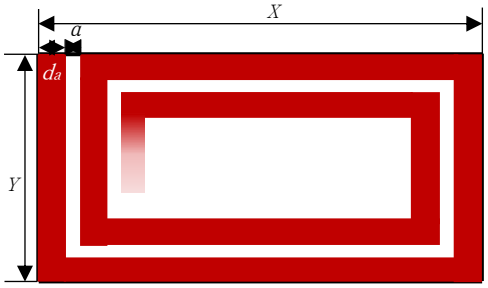

Fig. 11 Coil parameters

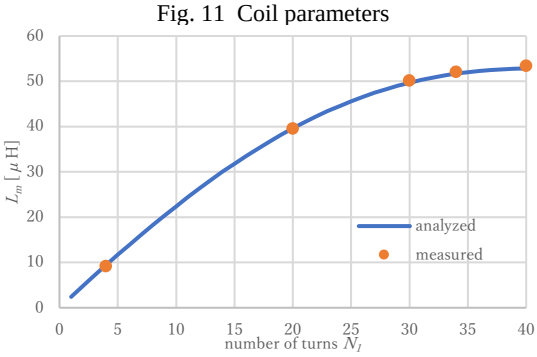

Fig. 12 Comparison between analyzed and measured values of mutual inductance L_m (N_2=30).

Fig. 12 shows the comparison between the analyzed and measured values when the number of turns of the secondary coil is 30. It can be seen that the analytical and measured values are in very good agreement.

3.4 STEP4

The internal resistance of the coil at each number of turns is derived from (11) and (12).

The comparison between the analyzed and measured values is shown in Fig. 13 and Fig. 14. The error became larger when the number of turns was increased. This may be due to the simple increase in the line length and the fact that only the external magnetic field up to the next line is considered for simplicity. It is said that it is difficult to derive the AC resistance of Litz wire, but this result captures the characteristics well.

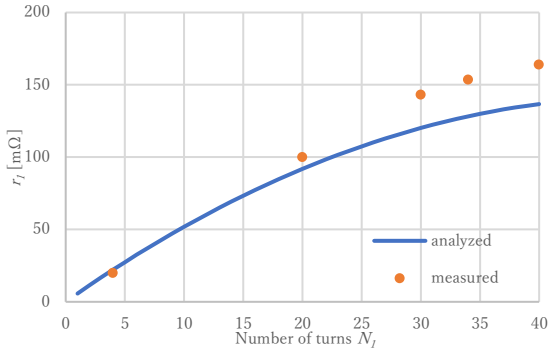

Fig. 13 Resistance of transmission coil

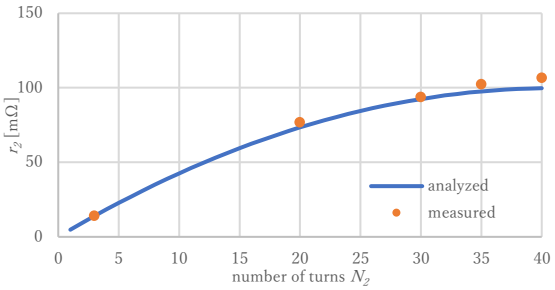

Fig. 14 Resistance of the receiving coil

3.5 STEP5

The kQ product was obtained from the mutual inductance L_m and internal resistance r_i obtained in STEP3 and STEP4 using (6). The simulation results are shown in Fig. 15 and Fig. 16. The maximum kQ product was obtained for 34 turns on the primary side and 30 turns on the secondary side, resulting in the maximum efficiency η_{max}.

Next, we compare the analyzed and measured values. The comparison between the measured and analyzed values was made along the black line in the figure, and the position of the graph adopted for this paper is plotted. The orange points are the

maximum points. Fig. 17 and Fig. 18 shows the relationship between the number of turns on the primary side and the *kQ* product and efficiency when there are 30 turns on the secondary side.

As in the analysis, the maximum *kQ* product was obtained for 34 turns on the primary side and 30 turns on the secondary side, and the maximum efficiency was obtained. This means that the optimization to maximize the efficiency within the given coil size was achieved.

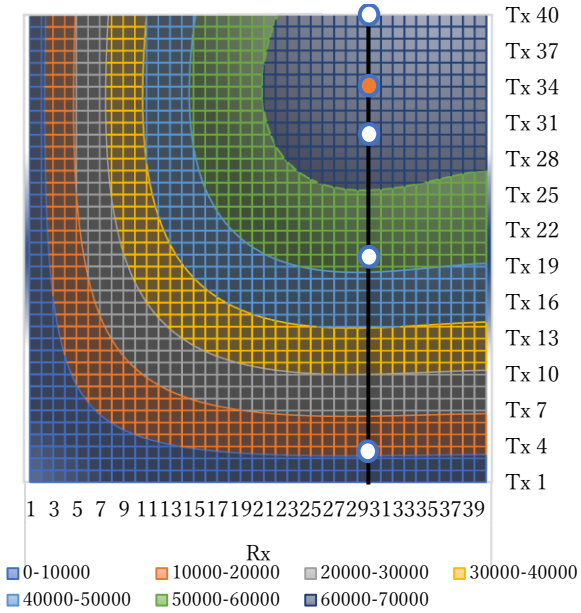

Fig. 15 *kQ* product at each number of turns (No misalignment)

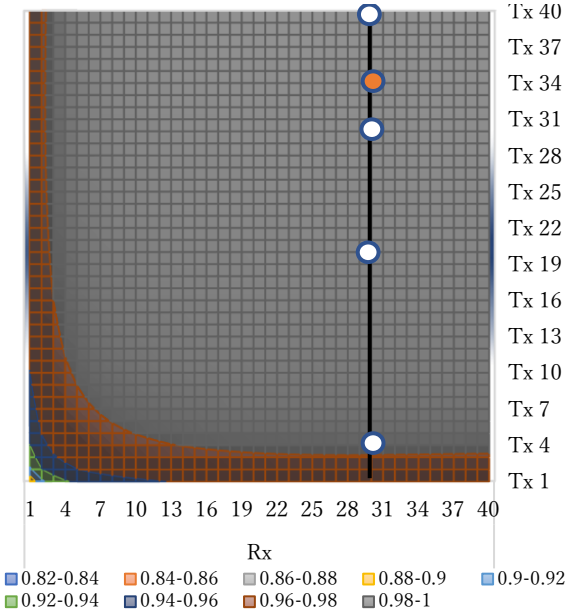

Fig. 16 Maximum efficiency η_{max} an each number of turns (No misalignment)

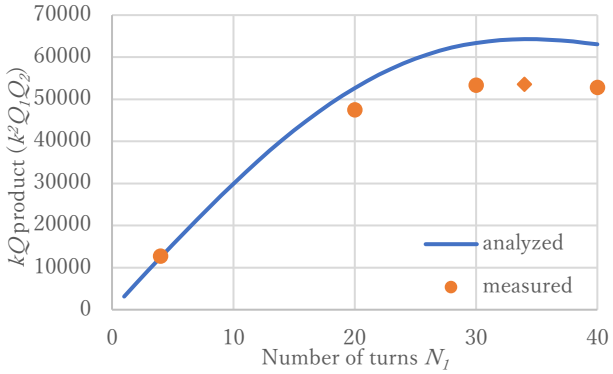

Fig. 17 *kQ* product at each number of turns at 30 on the secondary side. (◇: maximize of *kQ* product)

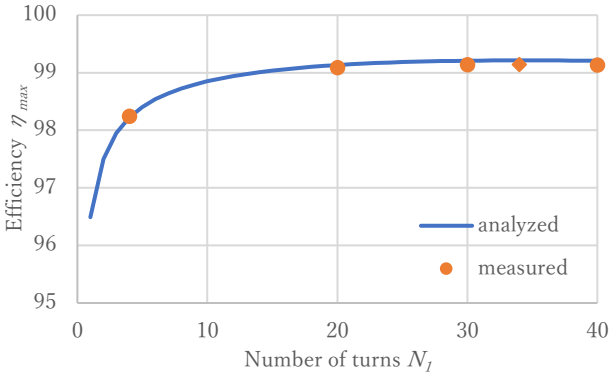

Fig. 18 Efficiency η_{max} at number of turns at 30 on the secondary side. (◇: maximize of efficiency)

4. MISALIGNMENT

In this section, the optimal coil in the case of misalignment was verified. The misalignment values were set to 75 mm in the X-direction and 100 mm in the Y-direction, as specified in SAE J2954, and we verified that the efficiency target of 80% was achieved.

The results of the analysis of *kQ* product and efficiency are shown Fig. 19 and Fig. 20. The comparison between the measured and analyzed values was made along the black line in the figure, and the position of the graph adopted for this paper is plotted. The orange points are the maximum points.

The maximum *kQ* product and efficiency η_{max} were obtained when the number of turns in the primary side was 33 and the number of turns in the secondary side was 29. Since we did not make a coil with 33 turns on the transmission side and 29 turns on the receiving side, we compared the measured values with the analyzed values using the same coil.

Fig. 21 shows the measurement scene. Fig. 22 and Fig. 23 shows the relationship between the number of turns on the primary side and the *kQ* product and efficiency when there are 30 turns on the secondary side.

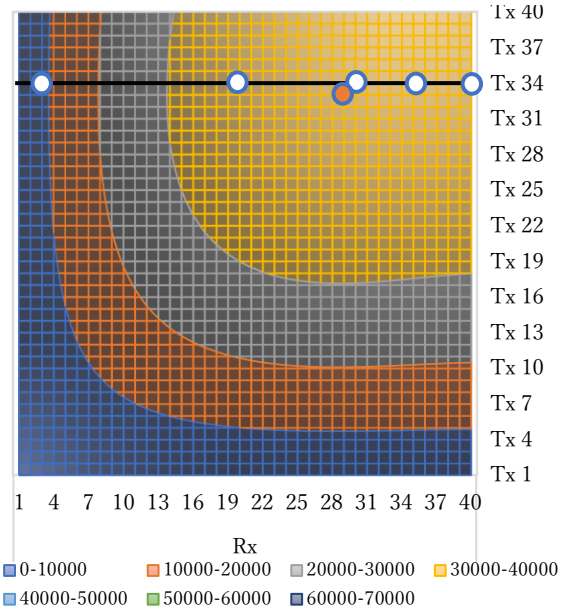

Fig. 19 *kQ* product at each number of turns (Misalignment ΔX=75, ΔY=100mm)

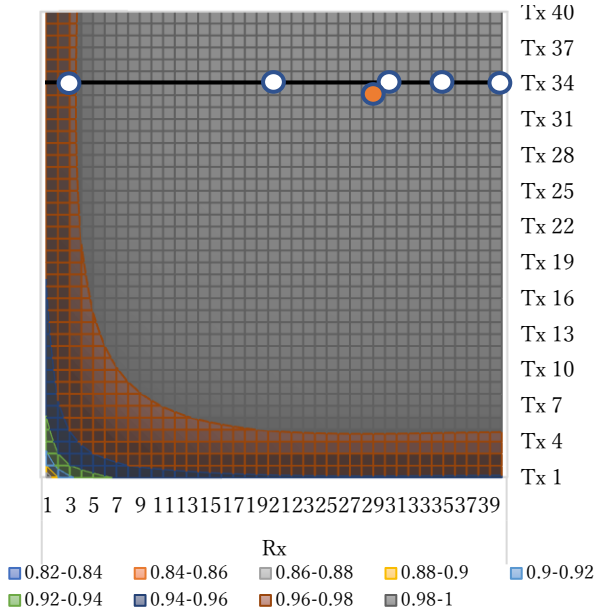

Fig. 20 Maximum efficiency η_{max} an each number of turns (Misalignment ΔX=75, ΔY=100mm)

Fig. 21 Measurement scene (Misalignment ΔX=75, ΔY=100mm)

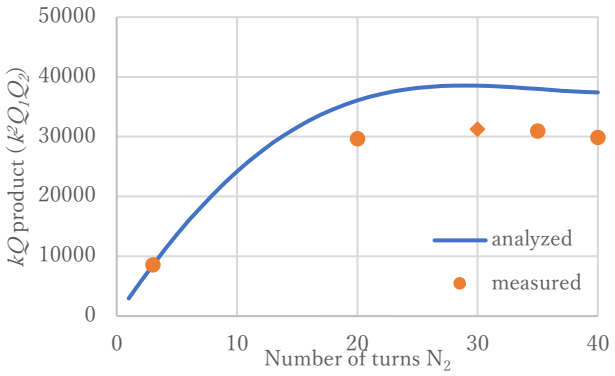

Fig. 22 *kQ* product at each number of turns at 34 on the primary side. (◇: maximize of *kQ* product)

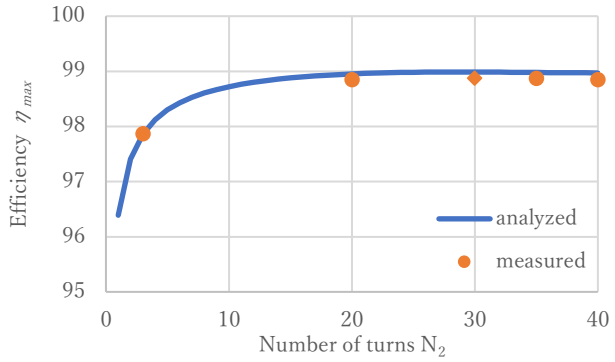

Fig. 23 Efficiency η_{max} at number of turns at 34 on the primary side. (◇: maximize of efficiency)

From the Fig. 22 and Fig. 23, it can be seen that the optimum coil designed for the case with no misalignment is almost the same as the optimum coil designed for the case with no misalignment.

The optimal coil with 34 turns on the primary side and 30 turns on the secondary side was also verified when the misalignment was increased. As shown in the Fig. 24, there was a null point, but it was found that 82% efficiency could be obtained even at 400mm in the X-direction and 75mm in the Y-direction. Fig. 25 shows the measurement scene at this misalignment. Even though we used an air-core coil this time, it proved to be strong for misalignment.

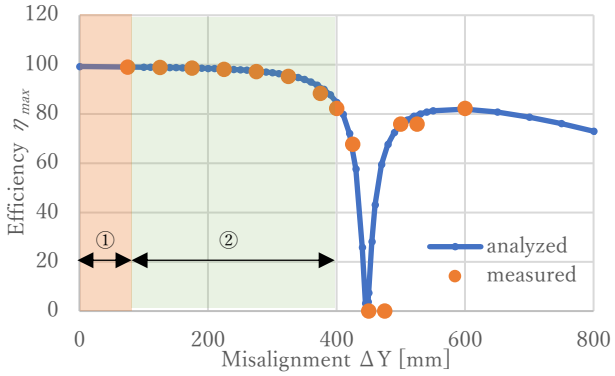

Fig. 24 Relationship between efficiency and ΔX (ΔY =100mm) (① : Within SAE standard, ② : Over 80%)

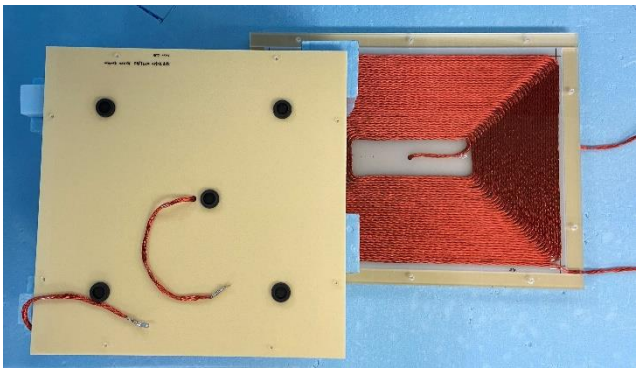

Fig. 25 Measurement scene
(Misalignment ΔX=400, ΔY=100mm)

5. CONCLUSION

In this study, we proposed a coil design method that achieves high efficiency only by numerical analysis without using electromagnetic field analysis. In addition, an optimum coil design method is proposed under the more practical conditions of SAE J2954. The proposed coil can achieve an efficiency of 99.2% without misalignment. In Chapter 4, we showed that the optimal coil design in the case of no misalignment is also nearly optimal in the case of misalignment within a specified range. The efficiency in the case of misalignment was very high, 98.8% even within the default range, and could be maintained above 80% even when the misalignment was 400 mm in the X-direction and 100 mm in the Y-direction. This proposal is based on the assumption that the coil is used for power supply while the electric vehicle is stopped, but it can be applied to all kinds of coils, not only coils used for power supply while the electric vehicle is running, and is very promising. In the future, we will examine the actual power used, the ferrite laying, and the compatibility of various coil combinations.

ACKNOWLEDGMENT

This work was supported by JSPS KAKENHI Grant Number 18H03768.

REFERENCES

[1] S. Li and C. C. Mi, "Wireless Power Transfer for Electric Vehicle Applications," in IEEE Journal of Emerging and Selected Topics in Power Electronics, vol. 3, no. 1, pp. 4-17, Mar. 2015.

[2] K. W. Klontz, D. M. Divan, D. W. Novotny and R. D. Lorenz, "Contactless battery charging system," US Patent 5157319, 1991.

[3] Y. J. Jang, S. Jeong and Y. D. Ko, "System optimization of the On-Line Electric Vehicle operating in a closed environment", ScienceDirect, Comput. Ind. Eng., vol. 80, pp. 222-235, Feb. 2015.

[4] O. C. Onar, J. M. Miller, S. L. Campbell, C. Coomer, C. P. White and L. E. Seiber, "A novel wireless power transfer for in-motion EV/PHEV charging," 2013 Twenty-Eighth Annual IEEE Applied Power Electronics Conference and Exposition (APEC), Long Beach, CA,

[5] R. Tavakoli and Z. Pantic, "Analysis Design and Demonstration of a 25-kW Dynamic Wireless Charging System for Roadway Electric Vehicles", IEEE Journal of Emerging and Selected Topics in Power Electronics, Sep 2018.

[6] H. Fujimoto, O. Shimizu, S. Nagai, T. Fujita, D. Gunji and Y. Ohmori, "Development of Wireless In-wheel Motors for Dynamic Charging: From 2nd to 3rd generation," IEEE PELS Workshop on Emerging Technologies: Wireless Power (WoW), Korea, pp. 56-61, 2020.

[7] K. Sasaki, T. Imura, “Combination of Sensorless Energized Section Switching System and Double-LCC for DWPT,” 2020 IEEE PELS Workshop on Emerging Technologies; Wireless Power Transfer (WoW), nov.2020.

[8] K. Hata, T. Imura and Y. Hori, "Simplified measuring method of kQ product for wireless power transfer via magnetic resonance coupling based on input impedance measurement," IECON, Beijing, China, pp. 6974-6979, 2017.

[9] Y. Suita, T. Imura, " Wireless Power Transfer Coil Design Method for High Efficiency by Theoretical Formula and Numerical Analysis," IEEJ , Mar. 2020.

[10] T. Mizuno, S. Enoki, T. Asahina, T. Suzuki, M. Noda and H. Shinagawa, "Reduction of Proximity Effect in Coil Using Magnetoplated Wire," in IEEE Transactions on Magnetics, vol. 43, no. 6, pp. 2654-2656, June 2007.

[11] R. Bosshard and J. W. Kolar, "Multi-Objective Optimization of 50 kW/85 kHz IPT System for Public Transport", IEEE Journal of Emerging and Selected Topics in Power Electronics, vol. 4, pp. 1370-1382, 2016.

[12] A. Namadmalan, B. Jaafari, A. Iqbal and M. Al-Hitmi, "Design Optimization of Inductive Power Transfer Systems Considering Bifurcation and Equivalent AC Resistance for Spiral Coils," in IEEE Access, vol. 8, pp. 141584-141593, 2020.

[13] SAE International, “Wireless Power Transfer for Light-Duty Plug-in/Electric Vehicles and Alignment Methodology J2954,” Issued2016-05, Revised2020-10.

[14] T. Imura, "Wireless Power Transfer : Using Magnetic and Electric Resonance Coupling Techniques," Springer, 2020.

[15] Y. Yazaki, T. Imura, H. Fujimoto, “Coil Design Method Considering with Required Specification for 85kHz Wireless Power Transfer System”, IEICT Technical Report, 2018.

[16] Jonas. Mühlethaler, “Modeling and Multi-Objective Optimization of Inductive Power Components”, DIS.ETH NO.20217, p.223, 2012.

[17] R. Y. Zhang, Jacob K. White, and John G. Kassakian, Charles R.Sullivan, ” Realistic Litz Wire Characterization using Fast Numerical Simulations”, in Applied Power Electoronics Conference and Exposition, pp.738‐745, 2014.

[18] C. R. Sullivan and R. Y. Zhang, "Simplified design method for litz wire", IEEE Applied Power Electronics Conference and Exposition (APEC), pp. 2667-2674, Apl. 2014.